Korea-Australia Rheology Journal
Vol. 16, No. 2, June 2004 pp. 63-73

Flow of a low concentration polyacrylamide fluid solution in a channel with a flat plate obstruction at the entry

M.A. Kabir, M.M.K. Khan* and M.G. Rasul
James Goldston Faculty of Engineering and Physical Systems, Central Queensland University, Rockhampton, Qld-4702, Australia

(Received September 9, 2002; final revision received February 4, 2004)

Abstract

Flow in a channel with an obstruction at the entry can be reverse, stagnant or forward depending on the position of the obstruction. These flow phenomena have potential applications in the control of energy and various flows in process engineering. Parameters that affect this flow inside and around the test channel are the gap (g) between the obstruction geometry and the test channel, the Reynolds number (Re) and the length (L) of the test channel. The influence of these parameters on the flow behavior was investigated using a flat plate obstruction at the entry of the channel. A low concentration polyacrylamide solution (0.018% by weight) showing a powerlaw fluid behavior was used as the fluid in this investigation. The flow phenomena were investigated by the velocity measurement and the flow visualization and their results were compared with numerical simulation. These results of low concentration polyacrylamide solution are also compared with the results of water published elsewhere (Kabir *et al.*, 2003). The maximum reverse flow inside the test channel observed was 20% – 30% of the outside test channel velocity at a g/w (gap to width) ratio of 1 for Reynolds numbers of 1000 to 3500. The influence of the test channel length (L) and the Reynolds number (Re) on the velocity ratio (V_i/V_o: inside velocity/outside velocity in the test channel) are also presented and discussed here.

Keywords : power-law fluid, reverse flow, forward flow, Reynolds number and test channel

1. Introduction

This work presents experimental investigation and numerical prediction of the flow of a low concentration polyacrylamide solution in a channel with obstruction at the entry, placed in another wider channel. The obstructed channel is referred to as the test channel. A recent study by Kabir *et al.* (2002) shows that the flow of a Newtonian fluid (water) inside a test channel with an obstruction at the entry placed in another wider parallel walled channel can be reverse, forward and stagnant depending on the different parameters. The parameters that influence the flow inside and around the test channel are the shape and size of the obstruction geometries, the gap (g) between the obstruction geometry and the test channel, the length (L) of the test channel and the Reynolds number (Re).

This flow phenomenon has potential benefits that can be employed in the control of energy and various flows in processing industries. Several applications where this type of flow phenomenon can occur or can be employed are: control of flow to obtain low velocities; heat transfer problems providing different types of flows locally; interaction of shear layer at varying distance apart; flow past obstruction and constrictions in arterial flows under certain physiological situations (Gowda *et al.*, 1989; Kabir *et al.*, 2002).

This flow behavior inside and around the test channel for water has attracted the attention of many researchers and has motivated authors to investigate the flow phenomena of non-Newtonian fluids as most industrial fluids exhibit non-Newtonian behavior. In most of the cases, polymer solutions and suspensions demonstrate non-Newtonian behavior. As a result, a low concentration polyacrylamide fluid solution exhibiting non-Newtonian behavior was chosen to investigate flow phenomena inside and around the test channel.

Despite the interesting nature of this flow, very limited research has been carried out with non-Newtonian fluids. There are, however, investigations using polymer solution (non-Newtonian fluid) where Liu (1999) studied the polymer liquid flow in a periodically constricted channel. Liu found that linear stability analysis in the inertial flow regime showed maximum destabilization in the diverging section of the periodic channel. Davidson *et al.* (1993) investigated the velocity and stress fields of polymeric liquids flowing in a periodically constricted channel.

*Corresponding author: m.khan@cqu.edu.au

Gowda and Tulapurkara (1989) carried out some investigation on the flow phenomenon of water in a channel at relatively low Reynolds number. Other studies have dealt with control of flow using different types of valves (Davis and Sorenson, 1969; Streeter, 1961; Eom, 1988; Hutchison, 1976). Bearman and Trueman (1972) investigated the flow around cylinders of different length to width ratio. Unal and Rockwell (1988a; 1988b) investigated the vortex shedding process and the influence of a splitter plate behind a circular cylinder. Bearman and Obasaju (1982) experimentally studied the pressure fluctuations on fixed and oscillating square-section cylinder. Mills *et al.* (1995) investigated the mechanism-controlling vortex shedding from rectangular bluff bodies.

An earlier investigation using water (Newtonian fluid) with different sizes and shapes of obstruction geometries, namely circle, triangle, rectangle and semicircle, found that flat plate produces the maximum reverse flow inside the test channel than any other obstruction geometry (Kabir *et al.*, 2002). Therefore, the flat plate was chosen as the obstruction geometry to study these flow phenomena with a non-Newtonian fluid.

The parameters chosen for this study were the gap (g) between the obstruction and the test channel, the length of the test channel (L) and the Reynolds number (Re) based on the channel width (w) and the outside velocity (V_o). These parameters were varied and their influences on the velocity ratios (V_i/V_o: inside velocity/outside velocity in the test channel) were studied.

The flow phenomena were investigated using the velocity measurement and the flow visualization technique and were compared with the numerical predictions. The velocity measurement technique provided the quantitative information of these flow phenomena, while the flow visualization technique provided the qualitative information. Flow visualization photographs were taken at the entry and exit ends of the test channel, capturing the important flow features at both ends. The CFD-ACE+ package was chosen for numerical predictions, which were later compared with the experimental results.

2. Experimental

2.1. Materials and equipment

The materials and equipment used were 0.018% (by weight) polyacrylamide fluid solution and a research grade Rheometer AR 1000-N. The additional materials and equipment used in this investigation were described in details elsewhere (Kabir *et al.*, 2003). A commercial CFD-ACE+ software package was chosen to use for numerical simulations.

2.2. Procedure

The experiment was carried out in an open channel rig designed and fabricated from galvanized steel sheet (Kabir *et al.*, 2002). The rig was equipped with the flow measurement and flow visualization instruments. The details of this open channel rig, the flow measurement and flow visualization technique are described elsewhere (Kabir *et al.*, 2003). The schematic diagram of experimental rig is shown in Fig. 1.

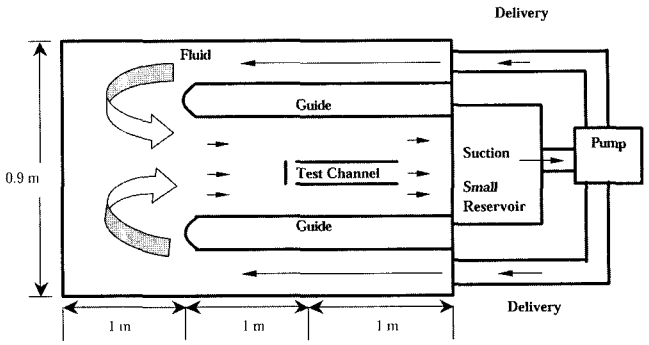

Fig. 1. Schematic diagram of experimental set up.

A low concentration non-Newtonian fluid solution was prepared by mixing 0.018% by weight of polyacrylamide (supplied by Cytec Australia Limited) powder with water. The solution was run through the pump for more than six hours for homogeneous mixing. To avoid any variation of the non-Newtonian fluid properties, the experiment was conducted at a constant temperature of 20°C. The rheological test of the fluid solution was carried out at 20°C, using a research grade Rheometer AR 1000-N. For all tests, the depth of the fluid in the channel was kept fixed at 130 mm.

Flow visualization pictures were taken using a Nikon Broadway high-speed digital camera. The exposure time of the photographs was 1/15 of a second. In this paper, the instantaneous flow visualization images are presented. However, it was observed in the test section of the rig and in the recorded video camera that flow pattern remain largely unchanged for the period of observation. Similar flow pattern was observed for water by Gowda *et al.* (1989). The authors had intended to compare them with the images of other flow visualization techniques such as PIV, but lack of other flow visualization techniques prevented them from doing so.

The overall flow in the test section of the open channel was observed steady. However, the flow was seen unsteady locally, particularly, at the entry and exit ends of the test channel. The most important flow features appeared to occur in the regions near the entry and exit of the test channel. To capture the flow field details of a manageable length, only entry and exit photographs were taken and a few are presented here.

The schematic diagram of the test arrangement is shown in Fig. 2. The width of the test channel (w) and breadth of the obstruction geometry (b) were 25 mm and kept con-

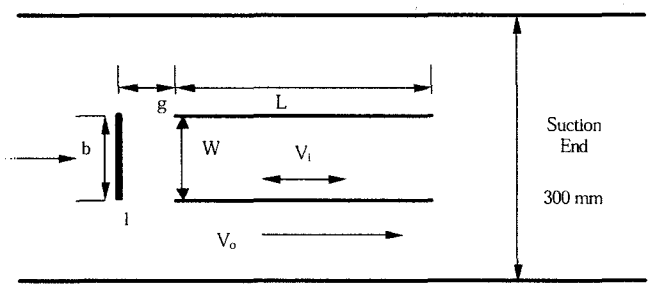

Fig. 2. Test channel arrangement.

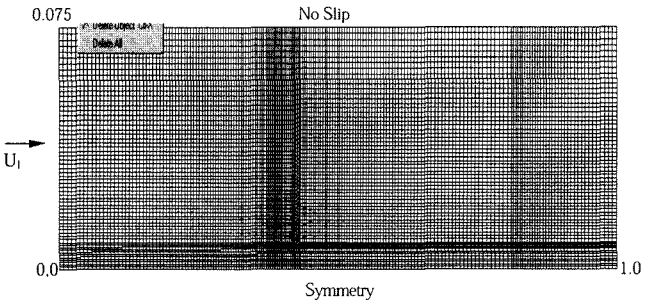

Fig. 3. Computational domains for the numerical prediction of flow.

stant. For this experiment, a flat plate obstruction was placed at the entry of the test channel. The length (l) to breadth (b) ratio (l/b) of the flat plate geometry was equal to 0.32. The flat plate obstruction geometry with l/b ratio of 0.32 was found to produce the maximum reverse flow (Kabir *et al.*, 2002) for Newtonian fluids (e.g. water) and was thus chosen for investigation into the influence of the gap (g) between the obstruction geometry and the test channel, the length (L) of the test channel, the Reynolds number (Re) on the velocity ratios (V_i/V_o). The gap (g) between the test channel and the obstruction was varied from 12.5 mm to 200 mm, giving a range of g/w ratios from 0.5 to 8. The investigation was carried out for test channel lengths (L) of 200 mm and 500 mm. The test was conducted for Reynolds numbers (Re) of 1000, 2000, 3000 and 3500 for each test channel length. The influence of the test channel length on the velocity ratio was investigated using different sets of test channel lengths. The influence of Reynolds number on the velocity ratio was also studied for test channel lengths of 200 mm and 500 mm.

3. Numerical simulation

Prediction of fluid flow processes can be obtained by two main methods: experimental investigation and theoretical calculations (Patankar, 1980). Besides the practical and theoretical approaches, numerical simulation has established itself in recent years as a third approach connecting the two traditional ones.

Computational Fluid Dynamics (CFD) modeling provides an alternative to laboratory experimentation by providing a relatively inexpensive, quick and accurate means of predicting flow behavior. The CFD-ACE simulation solver was chosen to study the flow parameters of the gap (g) between the test channel and the obstruction and the Reynolds number (Re).

The boundary conditions included no slip at the wall of the channel. The symmetry assumption was used so that the flow field would have to be solved for only the half of the test channel section.

The CFD-ACE+ code used was based on a finite volume method. The flow domain was discretized using unstructured grid. Computational flow simulations of this type are based on the division of the flow domain into small (finite) volumes. The domain used in this numerical prediction of flow phenomena is shown in Fig. 3. This is the same domain, used for experimental investigations of the flow phenomena of low concentration polyacrylamide solution inside and around a channel with obstruction at the entry. The flow inside and around the test channel was computed by solving the unsteady equations of motion for an incompressible power law fluid in a two-dimensional geometry. The continuity and momentum equations in dimensionless form can be written as

$$\frac{\partial u}{\partial x}+\frac{\partial v}{\partial y}=0.$$

$$\frac{\partial u}{\partial t}+u\frac{\partial u}{\partial x}+v\frac{\partial u}{\partial y}=-\frac{\partial p}{\partial x}+\frac{1}{Re}\left(2\left[\frac{\partial u}{\partial x}\right]^{n-1}\frac{\partial^2 u}{\partial x^2}+\left[\frac{\partial u}{\partial y}\right]^{n-1}\frac{\partial^2 u}{\partial y^2}+\left[\frac{\partial v}{\partial x}\right]^{n-1}\frac{\partial^2 v}{\partial x\partial y}\right)$$

$$\frac{\partial v}{\partial t}+u\frac{\partial v}{\partial x}+v\frac{\partial v}{\partial y}=-\frac{\partial p}{\partial y}+\frac{1}{Re}\left(2\left[\frac{\partial v}{\partial y}\right]^{n-1}\frac{\partial^2 v}{\partial y^2}+\left[\frac{\partial v}{\partial x}\right]^{n-1}\frac{\partial^2 v}{\partial x^2}+\left[\frac{\partial u}{\partial y}\right]^{n-1}\frac{\partial^2 u}{\partial x\partial y}\right) \quad (1)$$

The variables were made dimensionless as defined below by using U_i and w, followed by dropping the asterisks.

$$x^*=\frac{x}{w},\ y^*=\frac{y}{w},\ t^*=\frac{tU_i}{w},\ p^*=\frac{P}{\rho U_i^2},\ u^*=\frac{u}{U_i},\ v^*=\frac{v}{U_i},\ Re=\frac{U_i w\rho}{\mu}$$

Here U_i and w are the reference uniform velocity at the entry of the test channel and the reference length respectively; and μ is the dynamic viscosity; ρ is the density of the fluid, and Re is the Reynolds number.

Volume, boundary and initial conditions were given in CFD-ACE solver to study the flow behavior by solving the two dimensional equation of motion. The volume conditions were 1) low concentration polyacrylamide solution fluid for all domains except obstruction and test channel domain; 2) obstruction and test channel both domain are blockage. The boundary conditions were 1) no-slip condition on (a) top and bottom walls of the wider channel (b) walls of the test channel and (c) surfaces of obstruction; 2)

inlet velocity was kept at 0.115 m/s, 0.205 m/s and 0.24 m/s which gives Reynolds number of 1000, 2000 and 3000 respectively. The initial conditions for all domains were: velocities at u and v (x and y directions) were 10^{-6} m/s. Temperature taken was 20°C same as for the experimental investigation. Simulation results of the influence of the gap between the test channel and the obstruction are presented, compared and discussed with the experimental investigation.

3. Results and discussions

For a non-Newtonian fluid, if the shear stress, τ versus shear rate, $\dot{\gamma}$ plotted on log-log coordinates, follows a straight line over a range of shear rate, this part of the flow curve can be described by the following power law expression:

$$\tau = K\dot{\gamma}^{n} \tag{2}$$

Here K and n are the fluid consistency and power law index respectively.

$$\text{Or } \eta = K(\dot{\gamma})^{n-1} \tag{3}$$

Evidently, for pseudoplastic or shear thinning substance $n < 1$. The lower the value of n, the greater is the degree of shear thinning.

The rheological tests of the low concentration polyacrylamide fluid solution were carried out using a commercial rheometer type AR 1000 N and showed a shear thinning effect. The other rheological tests also showed that this fluid was fairly elastic and did not exhibit any yield stress. The shear rate range to which n and K values were obtained was narrow (0.5 to 10 sec^{-1}). The K and n values for the solution were determined from the response curve and were 3.223×10^{-3} $\text{Pa}\cdot\text{s}^{n}$ and 0.8337 respectively. These values were used in the power law model equation (3) to find out the viscosities η and used for experimental studies. Besides experimental studies, values of K and n were used in CFD solver for numerical simulation.

The shear rate or velocity gradient $\dot{\gamma}$ for open channel is given by $dv/dy = 2V_o/h$ (Vennard and Street, 1982) where V_o and h are the surface velocity outside the test channel and depth of the fluid respectively. By substituting the value of shear rate or velocity gradient $\dot{\gamma}$ in equation (3), the power law model equation can be written as:

$$\eta = K\left(\frac{2V_o}{h}\right)^{n-1} \tag{4}$$

The general formula for Reynolds number of Newtonian fluids is given by

$$Re = \frac{V_o w \rho}{\eta} \tag{5}$$

where w is the width of the test channel.

By substituting the viscosity, η from equation (4) in equation (5) the Reynolds number can be written as;

$$Re = \frac{V_o w \rho h^{n-1}}{K(2V_o)^{n-1}}$$

Or

$$Re = \frac{V_o^{2-n} w \rho h^{n-1}}{K(2)^{n-1}} \tag{6}$$

The flow parameters namely, the gap (g) between the test channel and the obstruction geometry, the Reynolds number (Re) and the length (L) of the test channel have significant effect in determining the flow behavior of polyacrylamide fluid solution inside and around the test channel. The influence of those parameters was investigated using velocity measurement and flow visualization photographs and was compared with the numerical predictions. The effect of the flow parameters on the velocity ratio (V_i/V_o: velocity inside/velocity outside the test channel) is presented and discussed below.

3.1. Effect of gap g

The gap (g) between the obstruction geometry and the test channel is one of the important flow parameters affecting flows inside and around the test channel. The influence of the gap (g) on velocity ratio (V_i/V_o) was seen to be significant and was studied for a range of Reynolds numbers from 1000 to 3500. The test channel lengths (L) used were 200 mm, 300 mm, 400 mm and 500 mm (L/w = 8, 12, 16 and 20), but only the results of test channel lengths (L) of 200 mm and 500 mm (L/w = 8 and 20) are presented for the sake of brevity. As mentioned earlier, the gap to width (g/w) ratio was varied from 0.5 to 8. The tests were carried out at g/w ratios of 0.5, 1, 1.5, 2, 3, 4, 5, 6, 7 and 8. For each g/w ratio, velocities (V_o) were varied from 0.115 to 0.3505 m/s, giving a range of Reynolds numbers from 1000 to 3500.

The influence of the gap to width g/w ratio on the velocity ratio (V_i/V_o) is shown in Figs. 4 and 5. A negative (−) value of the velocity ratio indicates a reverse flow, whereas a positive (+) value indicates a forward flow. At low g/w ratios ($g/w = 0.5$), the flow inside the test channel was found to be reverse and as g/w ratio increases magnitude of the reverse flow increases. The maximum reverse flow occurs at g/w ratio of 1 for Reynolds numbers of 1000, 2000, 3000 and 3500. With further increase in g/w ratio (g/w = 1.4), flow inside the channel was found to be stagnant for all Reynolds numbers except for Reynolds numbers of 1000 and 2000. For low Reynolds numbers (Re = 1000 and 2000), stagnation flow was seen at g/w ratio of 2.50 and 1.75 for L/w ratio of 8 as shown in Fig. 4. For L/w ratio of 20, as shown in Fig. 5, stagnation flow was seen at g/w ratio of 1.5 for all Reynolds numbers except Reynolds number 1000. For Reynolds number of 1000, stagnation

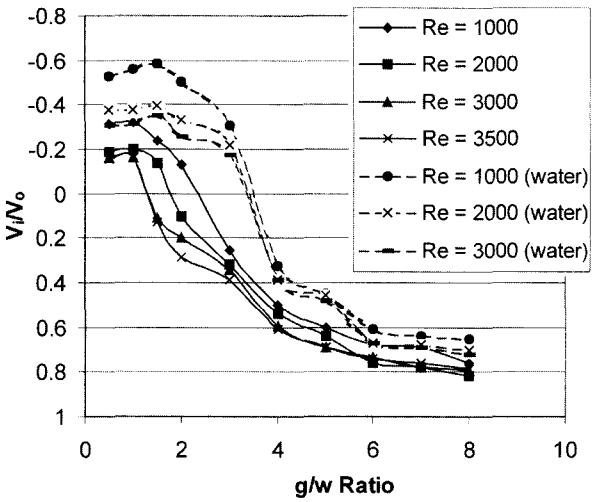

Fig. 4. Effect of gap on V_i/V_o ratio, $L/w = 8$ for polyacrylamide solution and water.

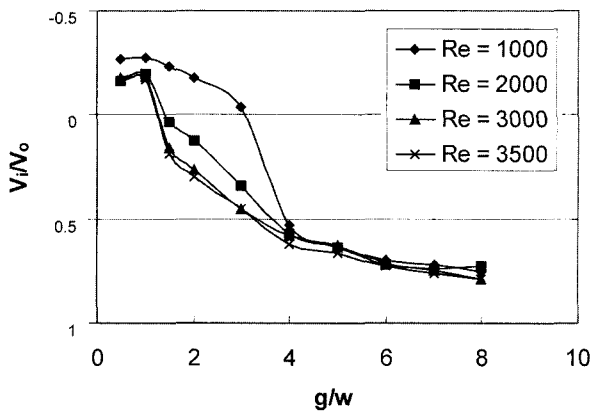

Fig. 5. Effect of gap on V_i/V_o, $L/w = 20$.

flow was seen at g/w ratio of 3.1. With further increase in g/w ratio the flow inside the test channel was observed to occur in the forward direction.

In flow with water, the maximum reverse flow was observed inside the test channel at g/w ratio of 1.5 as seen in Fig. 4 (Kabir *et al.*, 2002). The magnitude of the reverse flow in the test channel was 60%, 40% and 35% of the outside velocity for Reynolds numbers of 1000, 2000 and 3000 respectively. For 0.018% polyacrylamide solution, the maximum reverse flow was observed at g/w ratio of 1 and the magnitude of the reverse flow inside the test channel was 30%, 23% and 20% of the outside velocity for Reynolds numbers of 1000, 2000 and 3000.

For the maximum reverse flow, it can be seen from the Figs. 4 and 5 that there is a shift of g/w ratio position from 1.5 for water to 1.0 for polyacrylamide solution, largely due to the influence of non-Newtonian fluid. Furthermore, it is evident that the magnitude of the reverse flow of low concentration polyacrylamide solution was observed to be almost half of that of water. It is believed that elastic effect of polyacrylamide solution with high shear rate played a vital role in the significantly large reduction of the magnitude of reverse flow inside the test channel. In relative terms, elastic liquid shows a strong aversion to reverse flow than the Newtonian liquid and unidirectional flow is more evident. D. B. Boger and K. Walters (1993) observed similar flow pattern and reported that elastic fluids have more affinity to unidirectional flow and do not like to change the flow direction.

The maximum forward flow inside the test channel was observed 75% to 80% of the outside velocity at g/w ratio of 8 for polyacrylamide solution for Reynolds numbers ranging from 1000 to 3000, where as the maximum forward flow inside the test channel was seen to be 65% to 78% of the outside velocity at g/w ratio 8 for water in the same Reynolds number range.

The photographs of entry and exit ends were taken to capture and investigate the flow phenomena since the most important flow features occur at the entry and the exit ends. Photographs are presented in Fig. 6a-d. These photographs show the flow pattern for L/w ratio of 8.0 ($L = 200$ mm). Typical flow visualization photographs (Fig. 6a and 6b) of the reverse flow were taken at g/w ratios of 0.5 and 1.5 respectively for Reynolds number 1000. Likewise, Fig. 6c and 6d show a forward flow at g/w ratio of 4.0 and 6.0 for Reynolds number of 1000.

It can be seen in the flow visualization photographs of Fig. 6a and 6b that at small gaps (g/w ratio ranging from 0.5 to 1.5), shear layers separating from the edges of the flat plate tend to reattach the sidewalls of the test channel. These give rise to low pressures at the gap, triggering the flow in the reverse direction through the test channel. As the gap increases, the shear layers can then roll up into the gap, which reduces the magnitude of the negative pressure behind the flat plate obstruction. This causes the reverse flow to weaken, cease or change to forward flow for g/w ratios of 1.4 to 3.1.

The shear layers at the front and rear ends on both sides of the channel become unstable and roll up giving rise to complex vortex shedding. This vortex regulates the flow of the fluid solution through the channel. The magnitude of the reverse flow is determined by the combination of the low pressure behind the obstruction and the vortex shedding.

It was observed from the flow visualization pictures that vortices of polyacrylamide fluid solution were relatively larger in size than these observed for water (Kabir *et al.*, 2002). It is noted that no attempt had been made to measure the strength of the vortices of water and low concentration polyacrylamide solution due to lack of instrumental facilities.

Numerical predictions obtained for this flow conditions and at the gap (g) on the flow were carried out at various

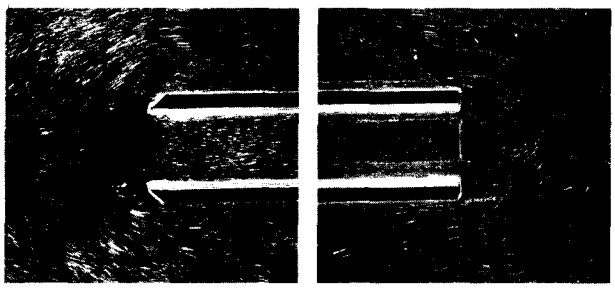

(a) g/w=0.5; Re=1000; L/w=8.0

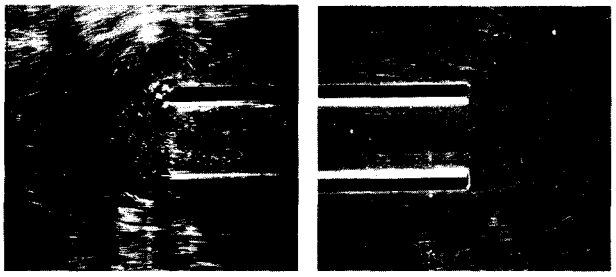

(b) g/w=1.5; Re=1000; L/w=8.0

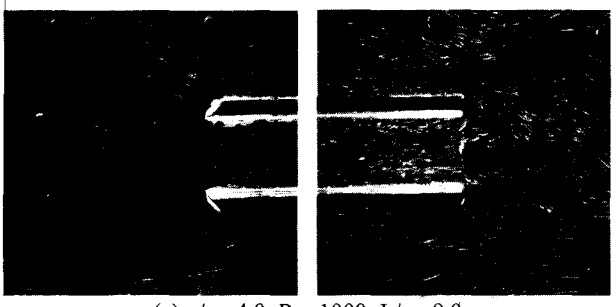

(c) g/w=4.0; Re=1000; L/w=8.0

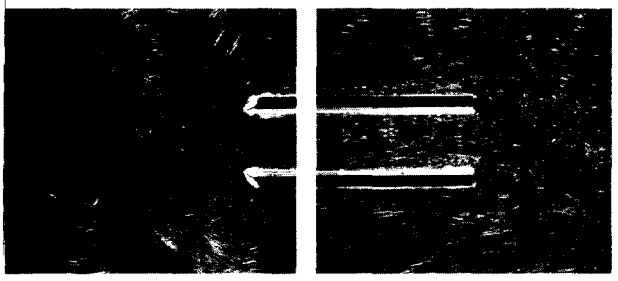

(d) g/w=6.0; Re=1000; L/w=8.0

Fig. 6a-d. Reverse flow pattern at *g/w* ratios of 0.5 an 1.5 (Fig. 6a-b) and forward flow pattern at *g/w* ratios of 4.0 and 6.0 (Fig. 6c-d).

g/w ratios of 0.5, 1.0, 1.5, 2.0, 3.0, 4.0, 5.0, 6.0, 7.0 and 8.0 for Reynolds number of 1000 and temperature of 20°C.

The numerically predicted results obtained by solving equation of motion for unsteady flow for low concentration polyacrylamide solution are generally in agreement with the experimental investigations. Although the numerical predictions were carried out for various *g/w* ratios, only the results of *g/w* ratios of 1.0 are presented and discussed for the sake of brevity. The selection of the case presented here was based on the experimental observations that maximum reverse flow occurs at *g/w* ratio of 1.0.

Several trials were made to eliminate the dependence of grid on the numerical simulation. The simulated streamline and the velocity vectors of the parameter are presented and discussed in Figs. 7. For better presentation of this flow parameter, the experimental flow visualization photographs, showing flow pattern inside and around the test channel, are presented at the top of those Figures, while the numerical predictions showing streamlines and velocity vectors are displaced at the bottom. The predicted numerical simulations are presented for the entry and exit ends of the test channel for comparison with the entry and exit ends of the experimental flow visualization photographs.

Case I. *g/w*- 1.0

Numerically predicted streamlines and velocity vectors at the entry and exit ends of the test channel are presented in Fig. 7(a-b) and 7(c-d) respectively at *g/w* ratio of 1.0, Reynolds number of 1000 and *L/w* ratio of 8.0. It can be seen from the streamlines and velocity vectors of the numerical simulation that the reverse flow inside the test channel matches exactly with the reverse flow of the experimental flow visualization photographs. The maximum reverse flow occurs at *g/w* ratio of 1.0. Numerically predicted value of the reverse flow inside the test channel is same as that of the experimental investigation of reverse flow found from velocity measurement. The numerical simulation of the gap (*g*) between the obstruction and the channel entry show good agreement with the experimental investigations at which maximum reverse flow occurs.

3.2. Effect of Reynolds number *Re*

The Reynolds number is another flow parameter that plays an important role in determining the nature of the flow inside and around the test channel. The influence of the Reynolds number on the magnitude of the velocity ratio (V_i/V_o) was investigated for a various set of test channel length (*L*) of 200 mm, 300 mm, 400 mm and 500 mm. For each test channel length, the gap (*g*) was varied from 12.5 mm to 200 mm, giving a *g/w* ratio of 0.5 to 8.0. For brevity, only the results of two test channel lengths of 200 mm and 500 mm (*L/w* = 8 and 20) are presented and discussed. Figs. 8 and 9 demonstrate the influence of Reynolds number on the velocity ratio (V_i/V_o) for *L/w* ratios of 8 and 20.

For lower *g/w* ratios, a strong reverse flow occurs at low Reynolds number for both *L/w* ratios of 8 and 20, as Reynolds number increases the reverse flow weakens and continues to decrease and then becomes almost stagnant, ultimately it turns stagnant with further increase in Reynolds number. For higher *g/w* ratios, the flow is forward for both *L/w* ratios and its value increases slightly with an increase in Reynolds number and becomes almost constant with further increase.

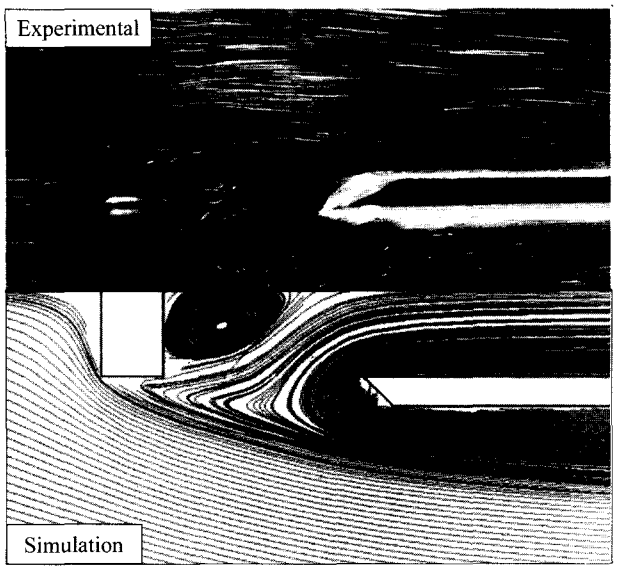

Fig. 7a. Predicted stream lines (bottom) and flow visualizatin photographs showing streak lines (top) at the entry of the test channel at g/w ratio of 1.0, time step = 55 for Re = 1000 and L/w = 8.0.

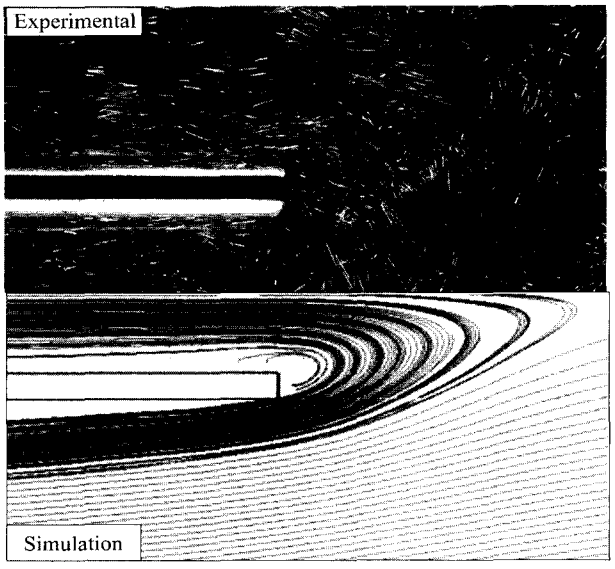

Fig. 7b. Predicted stream lines (bottom) and flow visualizatin photographs showing streak lines (top) at the exit end of the test channel at g/w ratio of 1.0, time step = 55 for Re = 1000 and L/w = 8.0.

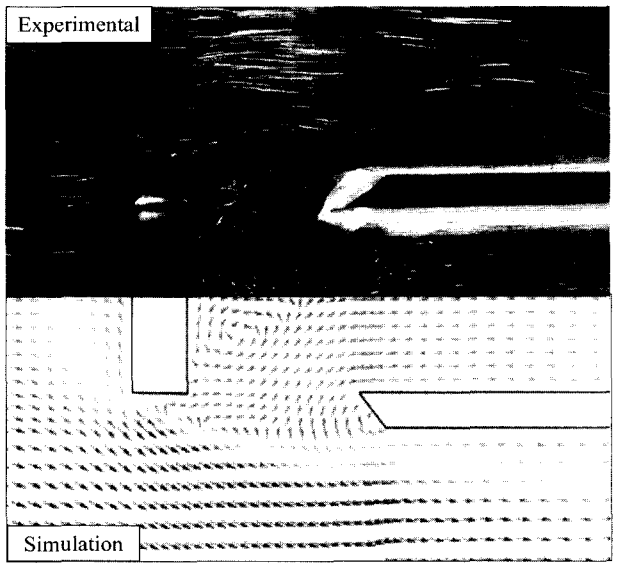

Fig. 7c. Predicted velocity vectors (bottom) and flow visualizatin photographs showing streak lines (top) at the entry of the test channel at g/w ratio of 1.0, time step = 55 for Re = 1000 and L/w = 8.0.

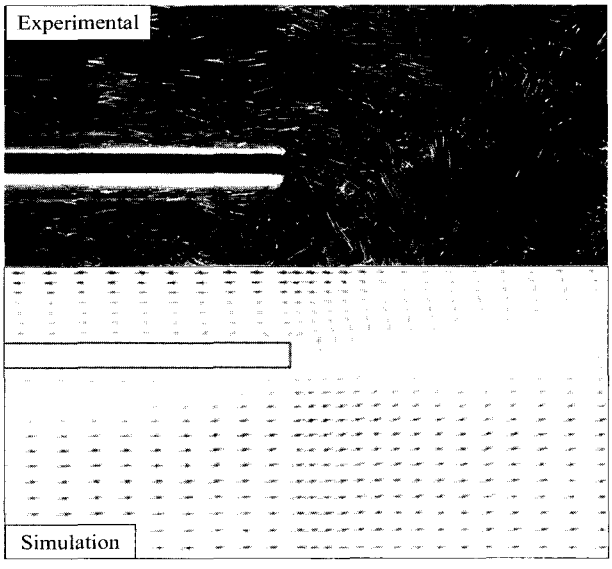

Fig. 7d. Predicted velocity vectors (bottom) and flow visualizatin photographs showing streak lines (top) at the exit of the test channel at g/w ratio of 1.0, time step = 55 for Re = 1000 and L/w = 8.0.

An interesting flow feature is noticed for g/w ratios of 1.5 and 2.0 for L/w ratio of 8. The reverse flow, observed at low Reynolds number, starts to weaken at 2000 and 1000 respectively, until it reaches to a stagnant flow at Reynolds numbers of 2500 and 1500 respectively. With further increase in Reynolds number the flow turns forward. Likewise, the reverse flow turns stagnant for g/w ratio of 1.5, 2.0 and 3.0 at Reynolds number of 700, 1500 and 2000 for higher L/w ratio of 20.

The reverse flow in the test channel, which was produced from the negative pressure behind the obstruction, was progressively neutralized as the gap (g) increases by the surrounding forward flow environment in the wider channel. At a certain position of the gap (g) between the obstruction and the test channel the reverse flow in the test channel was turned to stagnation.

Similar flow characteristics were observed for water flow for different L/w ratios. In the case of water for a L/w ratio

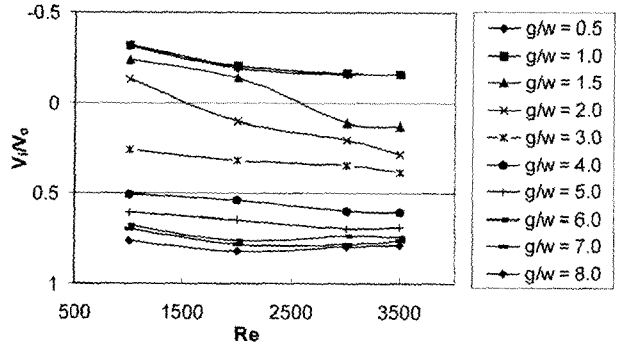

Fig. 8. Effect of Reynolds number on V_i/V_o, $L/w = 8.0$.

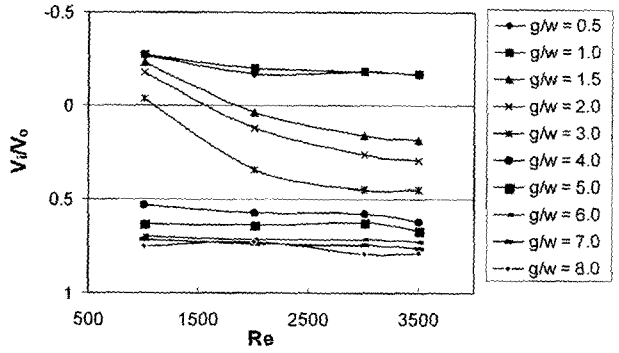

Fig. 9. Effect of Reynolds number on V_i/V_o, $L/w = 20$.

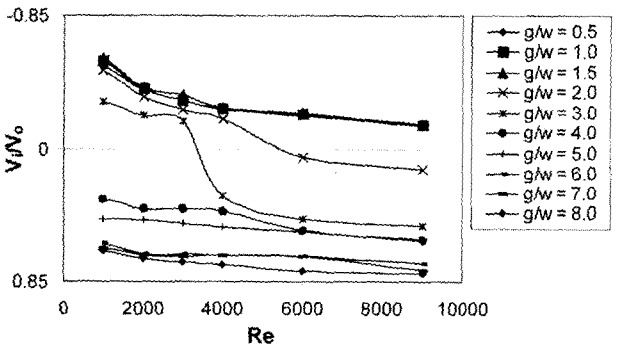

Fig. 10. Effect of Reynolds number on V_i/V_o ratio, $L/w = 8$ for water.

of 8, as can be seen in Fig. 10, the Reynolds numbers at which the reverse flows started to weaken were 4000 and 3000 at g/w ratios of 2 and 3 respectively. Stagnant flow conditions were observed at Reynolds numbers (Re) of 5500 and 3500. It is seen that there is a significant reduction in Reynolds numbers at which reverse flow began to weaken.

For the higher L/w ratio of 20, the reverse flow becomes stagnant for g/w ratios of 1.5, 2.0 and 3.0 at Reynolds numbers (Re) of 700, 1500 and 2000 respectively. When these results are compared with those of water (Kabir *et al.*, 2003), it is observed that the reverse flow inside the test channel starts to weaken and it reaches stagnation condition at significantly low Reynolds numbers (Re). The

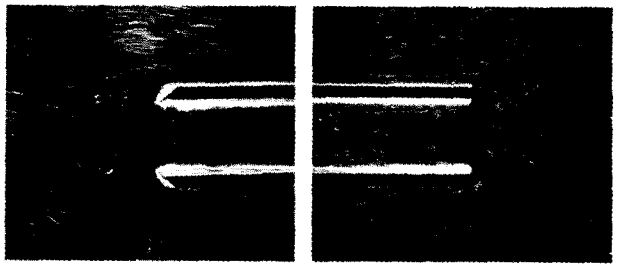

(a) Re=1000; g/w=1.0; L/w=8.0

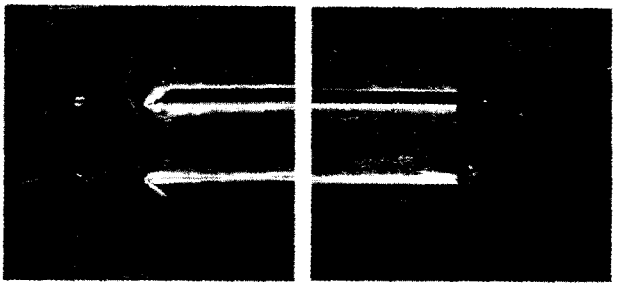

(b) Re=3000; g/w=1.0; L/w=8.0

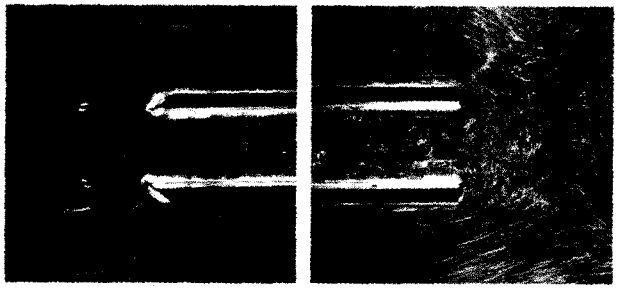

(c) Re=3500; g/w=1.0; L/w=8.0

Fig. 11a-c. Reverse flow pattern at different Reynolds number.

elastic behavior of the low concentration polyacrylamide solution fluid is believed to be responsible for the change of the above mentioned flow pattern.

The flow visualization photographs taken at Reynolds numbers of 1000, 2000, 3000 and 3500 are presented in Fig. 11a, 14a and 11b-c for L/w ratio of 8.0 and g/w ratio of 1.0. The vortices are clearly visible at both entry and exit ends, with increasing Reynolds number the vortex pattern changes at both ends.

It is known that two free shear layers, free to interact, are basically unstable and roll up to form discrete vortices. During the formation of the vortices and, to a much lesser extent, the shear layers draw in fluid from the base region. It is suggested that it is this continual entrainment process that sustains the low base pressure. The removal of entrained fluid is balanced by an induced reverse flow into the formation region. The base pressure determines the amount of vorticity that is being shed from each side of the body and this in turn is related in some way to the distance to vortex formation and the strength of the fully formed vortices (Bearman and Truemen, 1972).

After experimental investigations (velocity measurement

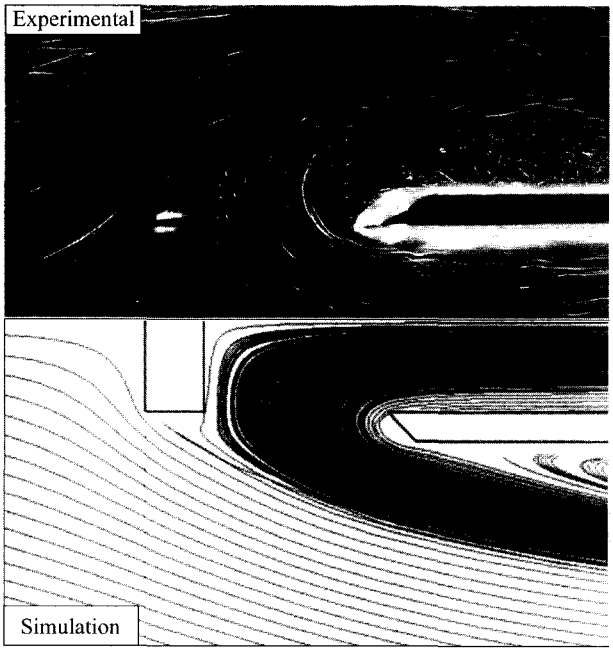

Fig. 12a. Predicted stream lines (bottom) and flow visualizatin photographs showing streak lines (top) at the entry of the test channel at g/w ratio of 1.0, time step of 55 for $Re = 3000$ and $L/w = 8.0$.

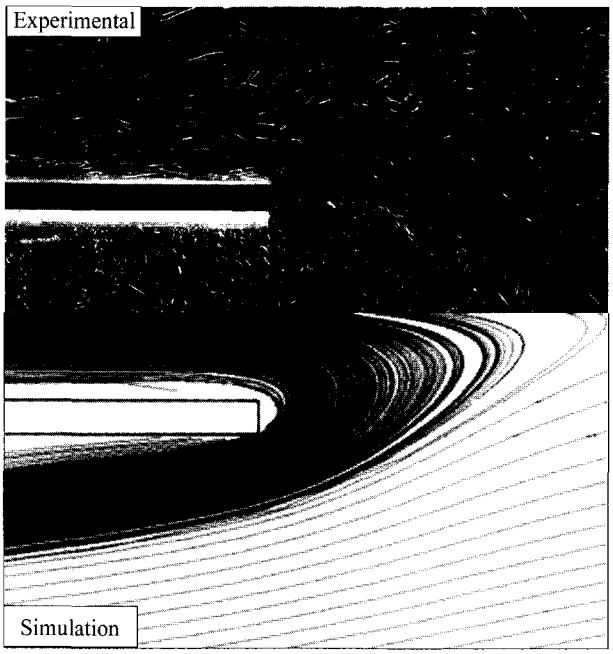

Fig. 12b. Predicted stream lines (bottom) and flow visualizatin photographs showing streak lines (top) at the exit end of the test channel at g/w ratio of 1.0, time step of 55 for $Re = 3000$ and $L/w = 8.0$.

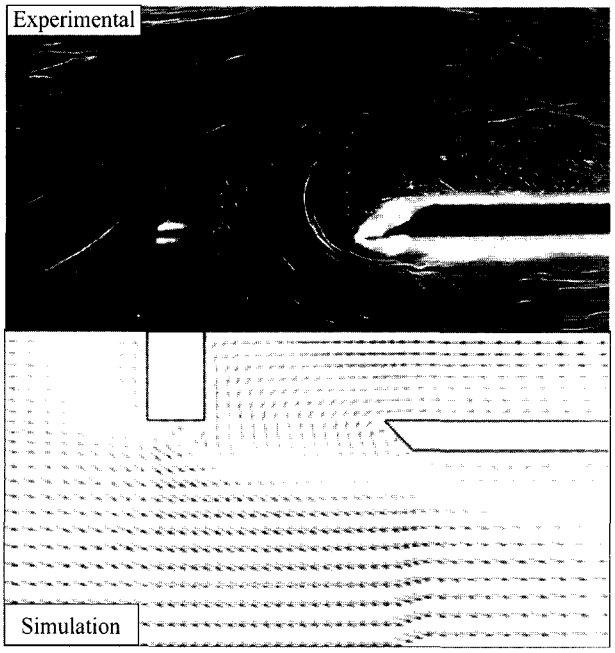

Fig. 12c. Predicted velocity vectors (bottom) and flow visualizatin photographs showing streak lines (top) at the entry of the test channel at g/w ratio of 1.0, time step of 55 for $Re = 3000$ and $L/w = 8.0$.

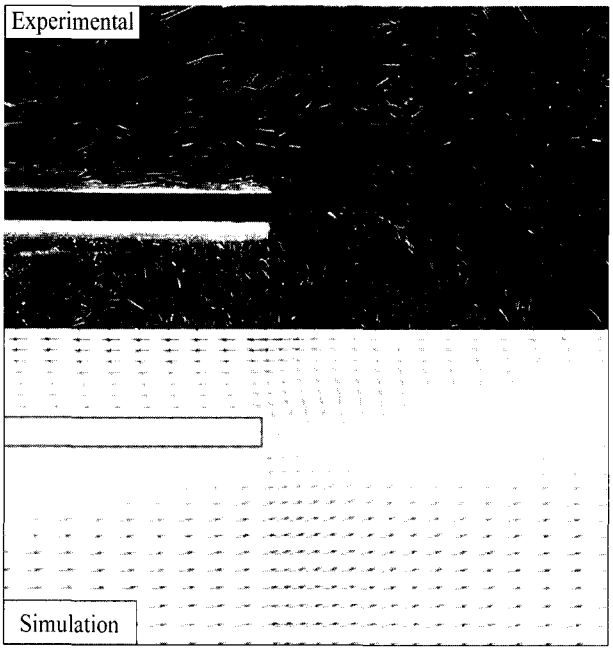

Fig. 12d. Predicted velocity vectors (bottom) and flow visualizatin photographs showing streak lines (top) at the exit end of the test channel at g/w ratio of 1.0, time step of 55 for $Re = 3000$ and $L/w = 8.0$.

and flow visualization) of the influence of Reynolds numbers, the authors intended to predict this flow parameter inside and around the test channel. The numerical prediction was carried out for a range of Reynolds numbers, from 1000 to 3000 for g/w ratio of 1.0 and L/w ratio of 8.0. It was found that the predicted values of the flow are in

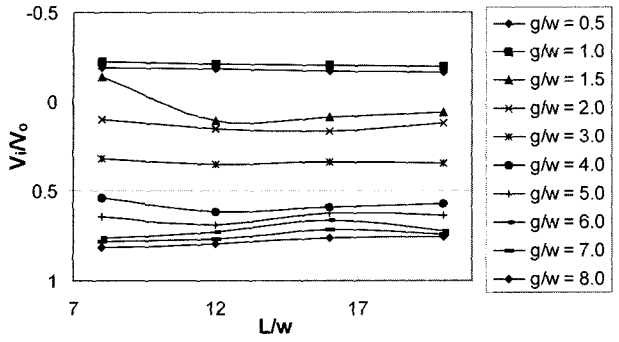

Fig. 13. Effect of length on V_i/V_o, $L/w = 2000$.

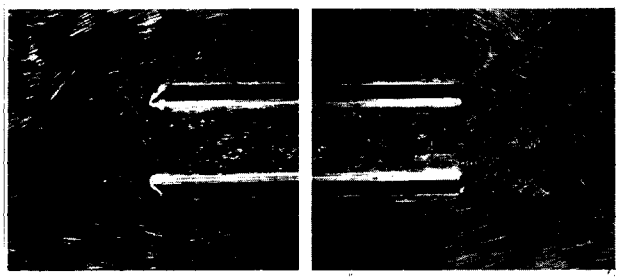

(a) L/w=8.0; Re=2000; g/w=1.0

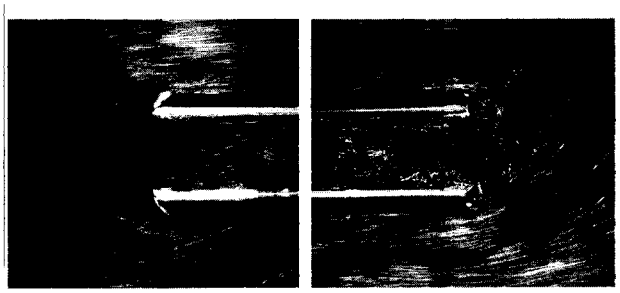

(b) L/w=20.0; Re=2000; g/w=1.0

Fig. 14a-b. Reverse flow pattern at different test channel length.

very good agreement with that of the experimental velocity measurement for Reynolds number ranging from 1000 to 3000. The predicted flow patterns are presented below the experimental flow visualization pictures for comparison (top part experimental picture and bottom part numerical prediction). The prediction showing streamlines and velocity vectors are compared with the streak lines of flow visualization photographs taken by digital camera and are presented in Figs. 7 and 12.

It is seen from the Figs. 7 and 12 that the predicted streamlines and velocity vectors showing vortices at the entry of the test channel are in good agreement with the flow visualization pictures showing streak lines vortices. The overall numerical predicted streamlines and velocity vectors showing reverse flow inside the test channel at Reynolds numbers of 1000 and 3000 match with the flow visualization pictures.

3.3. Effect of length *L*

The influence of the test channel length (L) on the velocity ratio (V_i/V_o) was investigated for g/w ratios ranging from 0.5 to 8.0. The experiment was carried out at the channel lengths (L) of 200, 300, 400 and 500 mm (L/w = 8, 12, 16 and 20). During the experiment, the velocity was kept constant at 0.215 m/s, giving a Reynolds number equal to 2000. Fig. 13 presents the influence of L on the velocity ratio for a range of g/w ratios.

It is observed that reverse flow occurs, at low L/w ratio (8 and 12) and a slight decrease in reverse flow occurs with increase in L/w ratio (16 and 20) for low g/w ratios of 0.5 and 1.0. Reverse flow inside the channel is caused by the low base pressure behind the obstruction geometry at the entry and it is expected that the velocity in the reverse direction would decrease slightly as the length of the test channel increases for g/w ratios of 0.5 and 1.0. For g/w ratio of 1.5, it was observed that the reverse flow at L/w ratio of 8 turns to stagnation flow at L/w of 10. With further increase in the L/w ratio, flow turned forward inside the test channel.

For g/w ratios of 2.0, 3.0 and 4.0, a forward flow inside the test channel was seen at low L/w ratio (8 and 12). The magnitude of the forward flow increases slightly as the L/w ratio (16 and 20) increases. For higher g/w ratios of 5.0, 6.0, 7.0 and 8.0, forward flow was observed at low L/w ratios and remains unchanged with further increase in L/w ratio.

Flow visualization pictures were taken at L/w ratios of 8 and 20 for Reynolds number 2000 and g/w ratio of 1.0 as shown in Fig. 14a-b. As seen, there is a slight change in flow pattern at the end of the test channel with increase in test channel length. In conclusion, it can be said that the length (L) of the test channel has very negligible influence on the flow inside the test channel.

4. Conclusion

Flow of a low concentration polyacrylamide solution fluid inside a channel with flat plate obstruction geometry and placed in another wider parallel walled channel was observed in forward, reverse and stagnant as expected. The parameters that affect the flow inside and around the test channel were the gap between the test channel and the flat plate obstruction, the length of the test channel and Reynolds number. Experimental investigations (velocity measurement and flow visualization techniques) and numerical prediction of the flow parameters are generally in good agreement. The maximum reverse flow inside the test channel was observed to be around 20% – 30% of the velocity outside the test channel, at a g/w ratio of 1.0 for Reynolds number ranging from 1000 to 3500, almost half of the magnitude of the reverse flow produced by water for same range of Reynolds numbers. The maximum forward flow was observed to be 80% of the outside test channel velocity at a high g/w ratio of 8.0, slightly higher than the

magnitude of the forward flow produced by water. At lower *g/w* ratios, the magnitude of the reverse flow was higher for low Reynolds numbers and a forward flow was observed at higher *g/w* ratio for a range of Reynolds numbers. The magnitude of this flow was determined by the combined effect of the low pressure behind the obstruction and the vortex shedding process at both entry and exit ends.

The magnitude of the reverse flow is higher at low Reynolds numbers and it deceases with an increase in Reynolds number for low *g/w* ratios. For higher *g/w* ratios, flow inside the test channel was observed to be in the forward direction and unaffected by the Reynolds number. The flow inside the test channel was almost unaffected by the length of the test channel for Reynolds number of 2000.

It can be concluded that the gap (g) between the test channel and the obstruction has the most significant influence on the velocity inside and around the test channel while Reynolds numbers have a moderate influence. The length of the test channel has little influence on the flow inside and around the test channel.

Acknowledgements

The authors gratefully acknowledge the support provided by the James Goldston Faculty of Engineering and Physical Systems, CQU, Australia to carry out the research work. Authors would like to thank Mr. Ray Kearney and Mr. Gary Hoare for their assistance in the fabrication of open channel rig, and Mr. Duncane Bourne and Dr. Col Greensil for their cooperation in the flow visualization photography.

References

Bearman, P.W. and E.D. Obasaju, 1982, An experimental study of pressure fluctuations on fixed and oscillating square-section cybers, *Journal Fluid Mechanics* **119**, 297-321.

Bearman, P.W. and D.M. Trueman, 1972, An investigation of the flow around rectangular cylinders, Aeronautical Quart, **23**, 229-237.

Bhuiyan, M.A., M.M.K. Khan and M.A. Kabir, 2000, Reverse flow of a non-newtonian fluid in a channel, Rheology Congress, Cambridge, U.K.

Boger, D.B. and K. Walters, 1993, Rheological Phenomena in Focus, Elsivier, New York.

Davidson, D., W.W. Graessley and W.R. Schowalter, 1993, Velocity and stress fields of polymeric liquids flowing in a periodically constricted channel, *Journal of Non-Newtonian Fluid Mechanics* **49**, 317-344.

Davis, C.G. and K.E. Sorenson, 1969, Handbook of applied hydraulics, Toranto, McGraw-Hill Co.

Eom, K., 1988, Performance of butterfly valves as a flow controller, *Journal of Fluids Engineering* **100**, 16-19.

Gowda, B.H.L. and E.G. Tulapurkara, 1989, Reverse flow in channel with an obstruction at the entry, *Journal of Fluid Mechanics* **204**, 229-244.

Hutchison, J.W., 1976, ISA Handbook of control valves.

Kabir, M.A., M.M. K. Khan and M.A. Bhuiyan, 2003, A study of the flow phenomenon of water in a channel with flat plate obstruction geometry at the entry, *KSME International Journal Korea* **17**, **6**, 879-887.

Kabir, M.A., M.M.K. Khan and M.G. Rasul, 2002, Flow of water in a channel with various obstruction geometries at the entry, The 2nd World Engineering Congress, Sarawak, Malaysia.

Liu, J., 1999, Stability of viscous and viscoelastic flows through periodically constricted channels, SIT, USA, 1-35.

Mills, R., J. Sheridan, K. Hourigan and M.C. Welsh, 1995, The mechanism controlling vortex shedding from rectangular bluff bodies, Twelfth Australiasian Fluid Mechanics Conference, The University of Sydney, Australia.

Patankar, S.V., 1980, Numerical heat transfer and fluid flow, Sydney, McGraw-Hill Book Company.

Streeter, V.L., 1961, Handbook of fluid dynamics, McGraw-Hill Co.

Unal, M.F. and D. Rockwell, 1988, On vortex formation from cylinder. Part 1. The initial instability, *Journal of Fluid Mechanics* **190**, 491-512.

Unal, M.F. and D. Rockwell, 1988, On vortex formation from cylinder. Part 2. Control by splitter-plate interference, *Journal of Fluid Mechanics* **190**, 513-292.

Vennard and Street, 1982, Elementary fluid mechanics, Brisbane, John Wiley and Sons.